Fabrication of trifunctional polyoxometalate hybrids for cascade conversion of glycerol targeting to lactic acid

Meilin Tao, Ningyue Sun, Yiming Li, Shengtian Wang, Xiaohong Wang*

Key Lab of Polyoxometalate Science of Ministry of Education, Northeast Normal University, Changchun 130024, P. R. China, E-mail: wangxh665@nenu.edu.cn, Fax: 0086-431-85099759

Materials.

All solvents and chemicals used were obtained from commercial suppliers. IR spectra (4000–500 cm^{-1}) were recorded on a Nicolet Magna 560 IR spectrometer (KBr discs). XRD patterns of the samples were collected on a Japan Rigaku Dmax 2000 X-ray diffractometer with Cu Ka radiation (0.154178 nm). TEM micrographs were recorded on a Hitachi H-600 transmission electron microscope. EDX spectra were obtained using 20 kV primary electron voltages to determine the composition of the samples. ^{13}C MAS NMR spectra of the samples were measured with a Bruker AVANCE III 400 WB spectrometer equipped with a 4 mm standard bore CPMAS probe with the X channel turning to 162 and 100.62 MHz, respectively. Elemental analysis was carried out using a Leeman Plasma Spec (I) ICP-ES and a PE 2400 CHN elemental analyzer. The critical micelle concentrations (CMC) of $Ly_{3-x}H_xPMo$ were measured by conductivity meter by break points of two nearly straight-line portions of the specific conductivity versus concentration.The redox potentials were tested by cyclic voltammetry (CV) on a CS Corrtest electrochemical workstation equipped with graphite powder (SP) and liquid paraffin (weight ratio = 4:1) as electrodes and saturated calomel as reference electrode. Electrochemical measurements were performed with 0.1 M sulfuric acid solution as the supporting electrolyte.Brunauer-Emmett-Teller (BET) surface area analysis was performed using the nitrogen adsorption isotherms using a NOVA 2000 series instrument, and the degas temperature was 90 ^oC. The H_2-TPR was tested by CHEMBET-3000. 5 % of H_2/Ar flow through the sample with a flow rate of 70 mL/min. The temperature progress was 30 ^oC to 500 ^oC with 10 ^oC/min, stay in 500 ^oC for 1 hour, and cooled down to the room temperature. The high performance liquid chromatography (HPLC) using a Shimadzu LC10A-VP chromatograph equipped with a SPB-10A Variable UV (210 nm) and a RID-10AR. I. detector. Prevail TM C18 column (4.6 mm × 250 mm). A solution of H_2SO_4 (0.1 % w/w) in H_2O/acetonitrile (1/2 v/v) (1.0 mL min-1) was used as the eluent at 50 °C.

Characterization of catalysts.

The IR spectra of as-prepared catalysts (Fig. S10) gave four characteristic peaks at 1083, 978, 900, and 795 cm^{-1}, which can be attributed to $\upsilon_{as}(P\text{-}O_a)$, $\upsilon_{as}(Mo\text{-}O_d)$, $\upsilon_{as}(Mo\text{-}O_b\text{-}Mo)$, and $\upsilon_{as}(Mo\text{-}O_c\text{-}Mo)$, respectively, and

these peakswere coincident with those of its parent $PMo_{12}O_{40}^{3-}$ (1080, 983, 890, 800 cm^{-1}). It indicated that the original Keggin structure of HPMo was retained after the participation of amino acid. Peaks at 1615, 1733 and 1489 cm^{-1} were due to the stretching bands of NH^{3+}, -COOH and C-N of lysine molecules, indicating the existence of lysine in the assembly spheres. There were little shifts of the bands of υ_{as}(Mo-O_d), υ_{as}(Mo-O_b-Mo), and υ_{as}(Mo-O_c-Mo), demonstrating the existence of the strong interactions between the HPAs and lysine. The blue shifts of NH_2 from 1710 to 1733 cm^{-1} proved that the NH_2 group of lysine is protonated as NH^{3+}. Therefore, the lysine cation and HPMo anion were combined through electrostatic effects.

The TEM image (Fig. S3) demonstrated that the $Ly_nH_{3-n}PMo$ materials could assemble colloid spheres with diameters from 5 to 10 nm. The Energy Dispersive X-ray (EDX) spectroscopy (Fig. S3) indicated that these hybrids were composed of $H_3PMo_{12}O_{40}$ and lysine, and the composition was evidenced by the presence of molybdenum, phosphorus, and carbon elements in the assemblies. The ratios of these elements from $Ly_xH_{3-x}PMo$ were given in table S1, which suggested the right compositions were prepared. This result also agreed with the results from the elemental analysis (table S2).

The critical micelle concentrations (CMC) of Ly_1H_2PMo, Ly_2H_1PMo, and Ly_3PMo were 0.60, 0.50 and 0.45 mM by break points of two nearly straight-line portions of the specific conductivity versus concentration (Fig. S4), which confirmed the formation of micelles in the aqueous solution.

The low-angle XRD patterns (Fig. S11) gave one Bragg diffraction peak appearing at 1.46, 1.22 and 1.04°, corresponding to Ly_1H_2PMo, Ly_2H_1PMo, and Ly_3PMo, respectively. The low-angle XRD showed that $Ly_xH_{3-x}PMo$ formed layered superstructures with layer spacings of 6.04, 7.27 and 8.48 nm, respectively.

As we can see from the ^{31}P NMR spectrum (Fig. S12), $H_3PMo_{12}O_{40}$ gave one peak at -4.812 ppm. While the peaks of -4.922, -5.024 and -5.112 ppm belonging to Ly_1H_2PMo, Ly_2H_1PMo, and Ly_3PMo, respectively, confirmed the formation of Keggin structure. The above results confirmed that the samples kept the Keggin structure after assembling. The change in chemical shift was attributed to the interactions between HPAs and Ly molecules.

Table S1 Elemental abundance for $Ly_xH_{3-x}PMo$from EDX.

	Ly_1H_2PMo		Ly_2H_1PMo		Ly_3PMo	
	atomic % (found)	stoichiometry (estimated)	atomic % (found)	stoichiometry (estimated)	atomic % (found)	stoichiometry (estimated)
C	10.01	6.3	16.44	12	21.59	18.0
N	3.09	1.9	5.58	4.1	7.33	6.1
P	1.59	1	1.37	1	1.20	1.0
Mo	19.01	11.9	16.54	12.1	14.66	12.2

Table S2. Elemental analysis, textural and chemical properties of $Ly_xH_{3-x}PMo$ catalysts.

	Ly_1H_2PMo	Ly_2H_1PMo	Ly_3PMo
	stoichiometry (estimated)	stoichiometry (estimated)	stoichiometry (estimated)
P	1 (1.0)	1 (1.0)	1 (1.0)
Mo	12.2 (12.0)	12.3 (12.0)	11.8 (12.0)
C	5.9 (6.0)	12.4 (12.0)	17.5 (12.0)
H	2.1 (2.0)	1.04 (1.0)	0 (0)
N	2.1 (2.0)	4.1 (4.0)	5.8 (6.0)
$S_{BET}(m^2/g)$	55.79	50.63	34.19
CMC(mM)	0.60	0.50	0.45
Redox potential (mV)	113.8	92.8	74.9

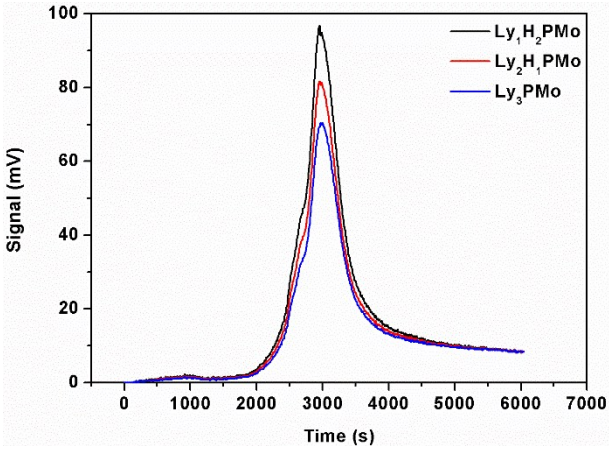

Fig. S1 The H_2-TPR spectra of $Ly_xH_{3-x}PMo$

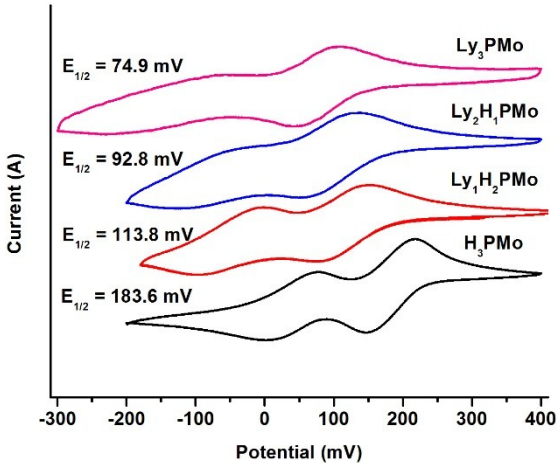

Fig. S2 The redox potentials of $Ly_xH_{3-x}PMo$: carbon paste (weight ratio = 1:3 of mineral oil and graphite) with 5 wt% POMs as working electrode, Pt wire as counter electrode, Ag/AgCl as reference electrode, 0.5 M KCl as electrolyte. Scan rate = 20 mV/s.

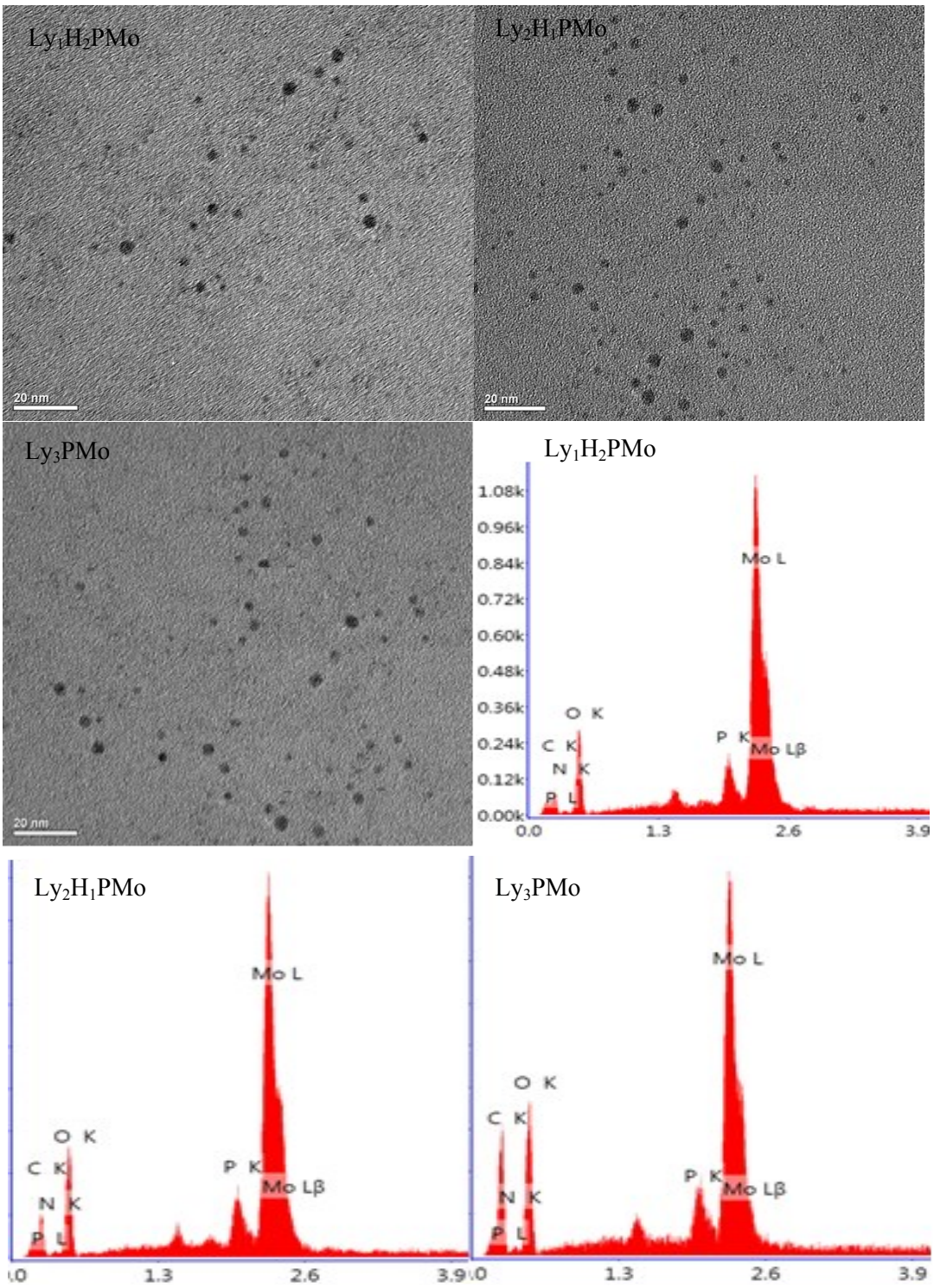

Fig. S3 TEM and EDX images of $Ly_xH_{3-x}PMo$

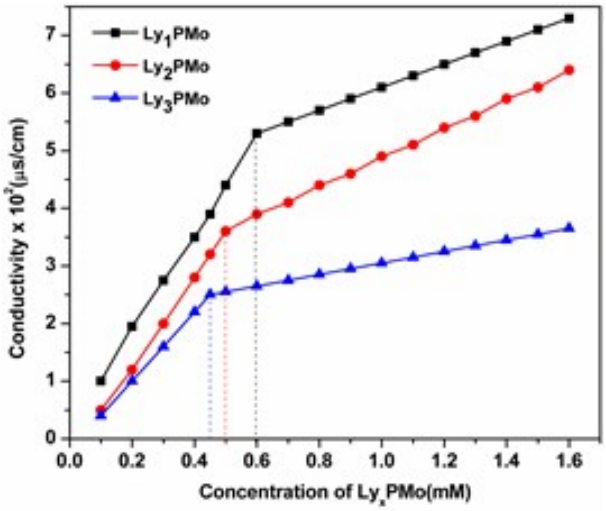

Fig. S4 The critical micelle concentrations (CMC) of $Ly_xH_{3-x}PMo$ at room temperature.

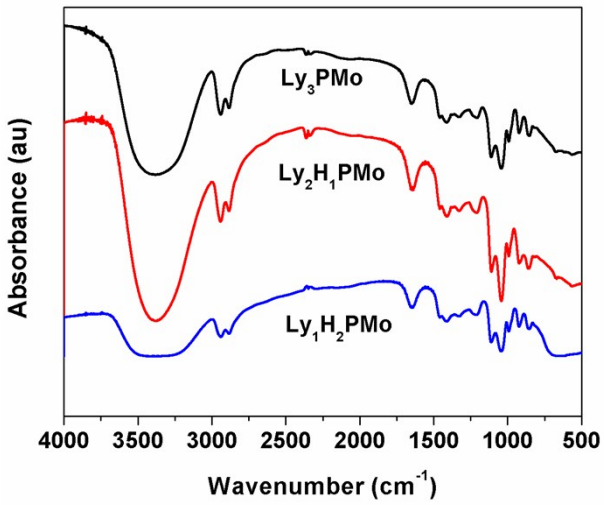

Fig. S5 The IR spectra of $Ly_xH_{3-x}PMo$ after absorbing glycerol.

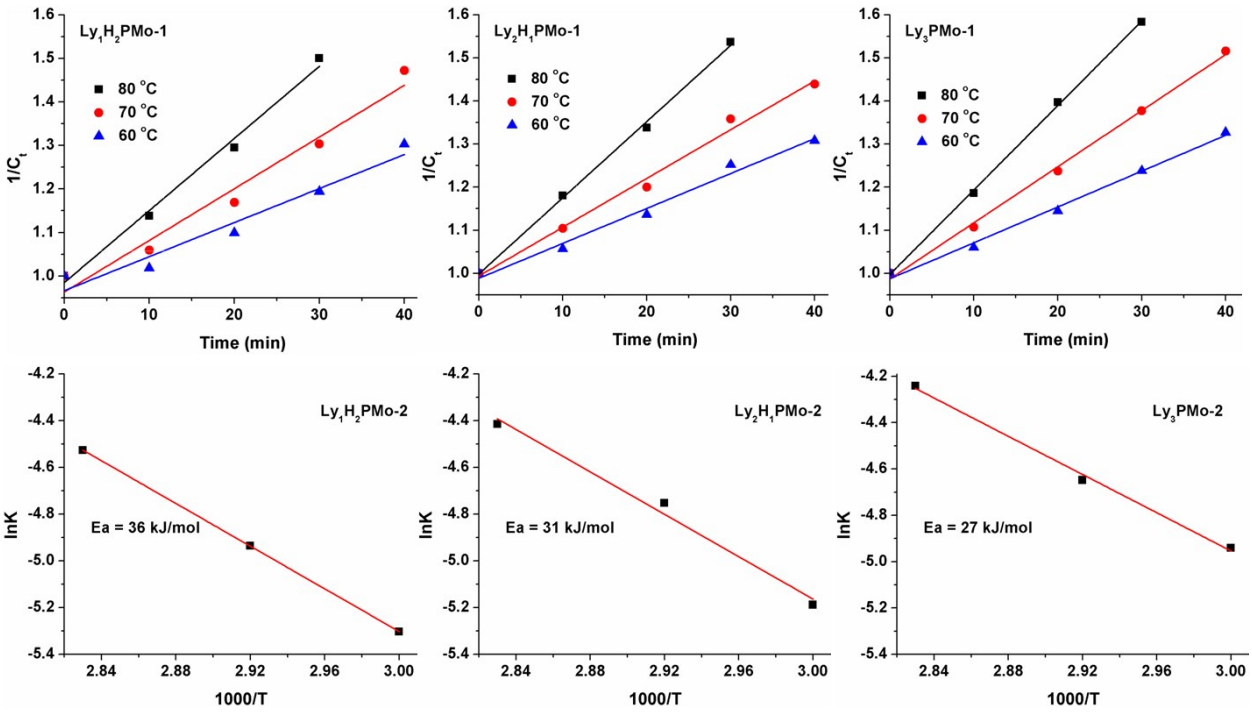

Fig. S6 The plots of the concentration of DHA versus reaction time ($1/C_t$-t curve) and the Arrhenius plots (lnK-t) over $Ly_xH_{3-x}PMo$ catalysts in the temperature range from 60 to 80 °C. (Ct: the concentration of glycerol with the reaction time)

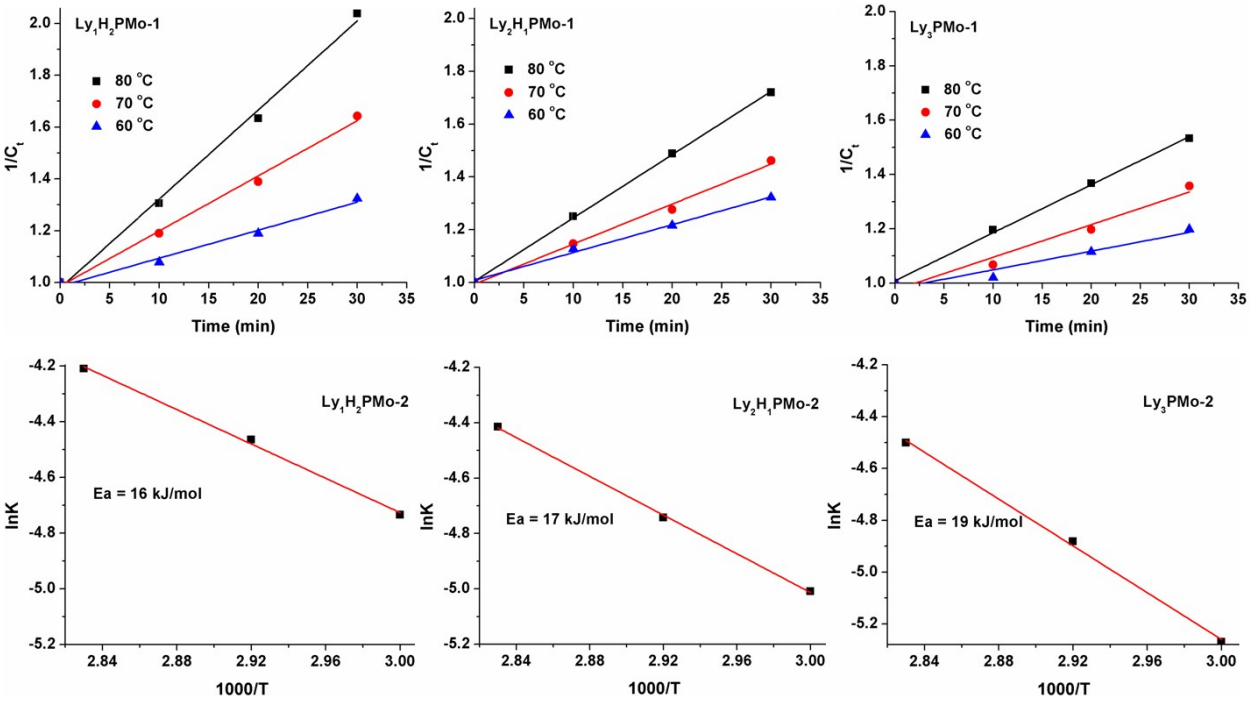

Fig. S7 The plots of the concentration of PRA versus reaction time ($1/C_t$-t curve) and the Arrhenius plots (lnK-t) over $Ly_xH_{3-x}PMo$ catalysts in the temperature range from 60 to 80 °C. (Ct: the concentration of glycerol with the reaction time)

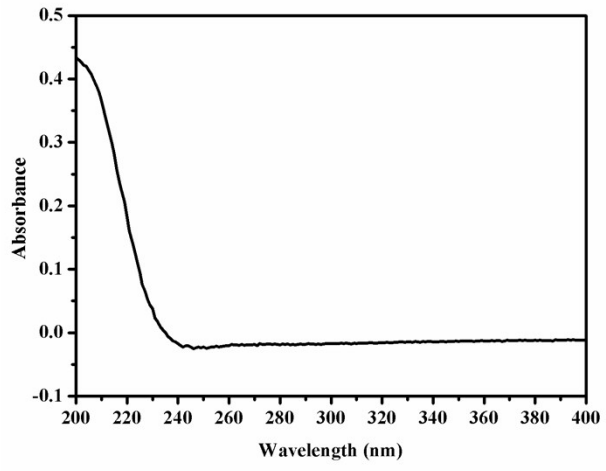

Fig. S8 The UV-vis spectrum of the reaction mixture after reaction being separated catalyst

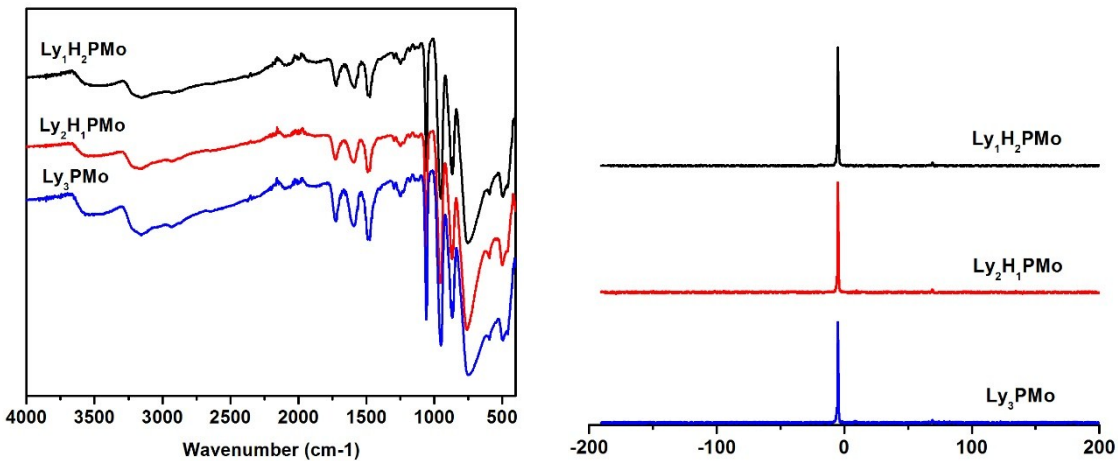

Fig. S9 The IR spectra and ^{31}P MAS NMR of $Ly_xH_{3-x}PMo$ after reaction.

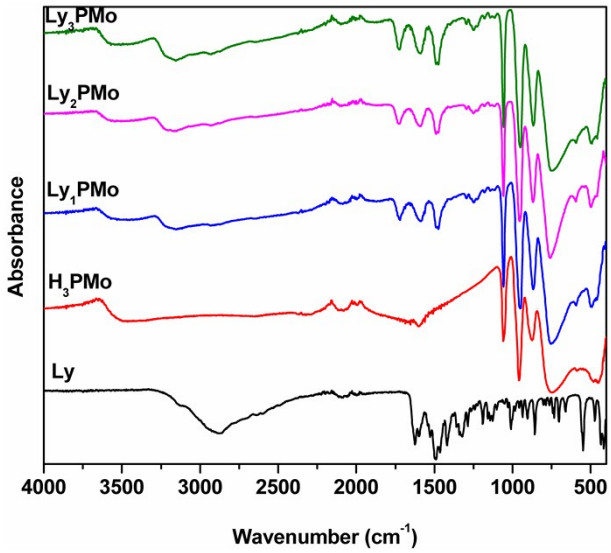

Fig. S10 The IR spectra of $Ly_xH_{3-x}PMo$ and lysine.

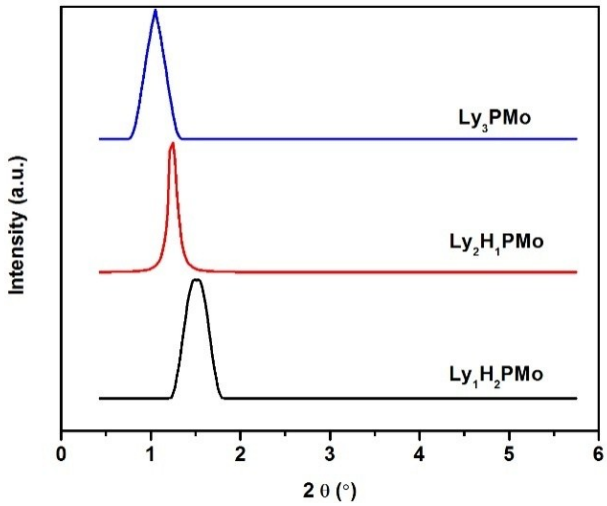

Fig. S11 Low-angle XRD patterns of $Ly_xH_{3-x}PMo$.

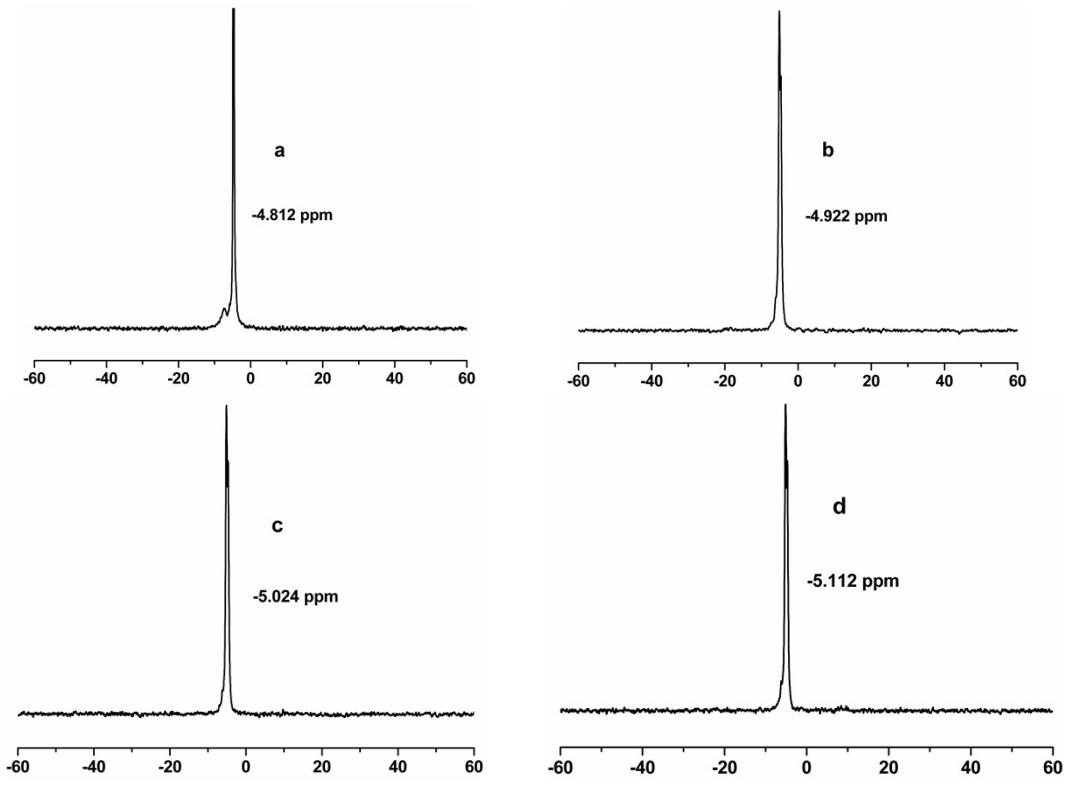

Fig. S12 The ^{31}P MAS NMR spectra of $Ly_xH_{3-x}PMo$: (a) x=0, (b) x=1, (c) x = 2, and (d) x = 3.